

A Novel Quantitative Multi-Component Serological Assay for SARS-CoV-2 Vaccine Evaluation

Morly Fisher, Alon Manor, Hagar Abramovitch, Ella Fatelevich, Yafa Afrimov, Gal Bilinsky, Edith Lupu, Amir Ben-Shmuel, Itai Glinert, Noa Madar-Balakirski, Hadar Marcus, and Adva Mechaly*



Cite This: *Anal. Chem.* 2022, 94, 4380–4389



Read Online

ACCESS |



Metrics & More

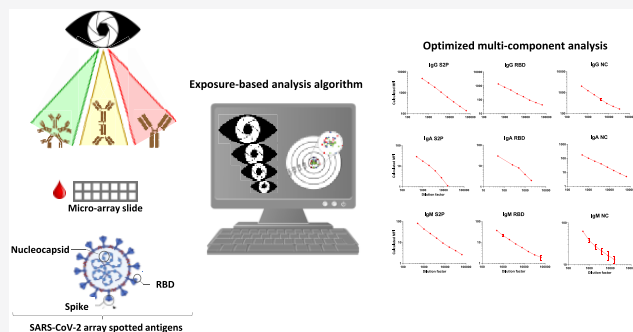


Article Recommendations



Supporting Information

ABSTRACT: A multi-component microarray, applying a novel analysis algorithm, was developed for quantitative evaluation of the SARS-CoV-2 vaccines' immunogenicity. The array enables simultaneous quantitation of IgG, IgM, and IgA, specific to the SARS-CoV-2 spike, receptor binding domain, and nucleocapsid proteins. The developed methodology is based on calculating an apparent immunoglobulin signal from the linear range of the fluorescent read-outs generated by scanning the microarray slides at different exposure times. A dedicated algorithm, employing a rigorous set of embedded conditions, then generates a normalized signal for each of the unique assays. Qualification of the multi-component array performance (evaluating linearity, extended dynamic-range, specificity, precision, and accuracy) was carried out with an in-house COVID-19, qRT-PCR positive serum, as well as pre-pandemic commercial negative sera. Results were compared to the WHO international standard for anti-SARS-CoV-2 immunoglobulins. Specific IgG, IgM, and IgA signals obtained by this array enabled successful discrimination between SARS-CoV-2 q-RT-PCR positive (seroconverted SARS-CoV-2 patients) and negative (naive) samples. This array is currently used for evaluation of the humoral response to BriLife, the VSV-based Israeli vaccine during phase I/II clinical trials.



INTRODUCTION

Severe acute respiratory coronavirus 2 (SARS-CoV-2) serology tests, along with qRT-PCR and rapid antigen tests, are part of the COVID-19 diagnostic landscape and thus play a pivotal role in disease management and containment.¹ At the initial stages of the pandemic, serological tests were used to determine SARS-CoV-2 prevalence in the community, discerning between naive and seroconverted individuals and were therefore mostly qualitative.² At the beginning of 2021, almost two years after the first diagnosed case of COVID-19, the Center for Disease Control and Prevention proclaimed that validated and standardized SARS-CoV-2 quantitative immunoglobulin assays are needed as part of the “next phase” response to the pandemic.³ This demand arises from the need to characterize the humoral response elicited by the different vaccines that are part of numerous vaccination campaigns around the globe. Despite this stipulation, only 15 out of about 100 FDA approved serology tests (<https://www.fda.gov/medical-devices/coronavirus-disease-2019-covid-19-emergency-use-authorizations-medical-devices/eua-authorized-serology-test-performance>, updated: 09/28/2021) are labeled as quantitative or semi-quantitative. Moreover, most of them detect only one immunoglobulin type aimed at a single viral protein,⁴ thus rendering them less suitable as analytical tools for vaccine evaluation.

We recently reported the development of a 6-plex antigen microarray that was applied for the characterization of seroprevalence and seroconversion in the Israeli adult population in the early stages of the COVID-19 pandemic in Israel.⁵ Based on the results and technical knowledge acquired during this effort, we developed a 3-plex array containing a stabilized version of the SARS-CoV-2 spike ectodomain (S2P), SARS-CoV-2 receptor binding domain (RBD), and the virus's nucleocapsid (NC), which is currently used for the characterization of the humoral immune response developed during clinical trials (phase I/II) of BriLife, the VSV-spike-based Israeli vaccine.⁶ Antibodies against the spike proteins (S2P and RBD) were found to correlate with neutralization⁷ and as such are considered essential for determining the vaccines' efficacy. Since this microarray is intended for periodic follow-ups of vaccinated volunteers, it is crucial to establish whether seroconversion is the result of vaccination or due to SARS-CoV-2 infection. The NC, spotted on the array, enables such

Received: December 6, 2021

Accepted: February 18, 2022

Published: March 1, 2022



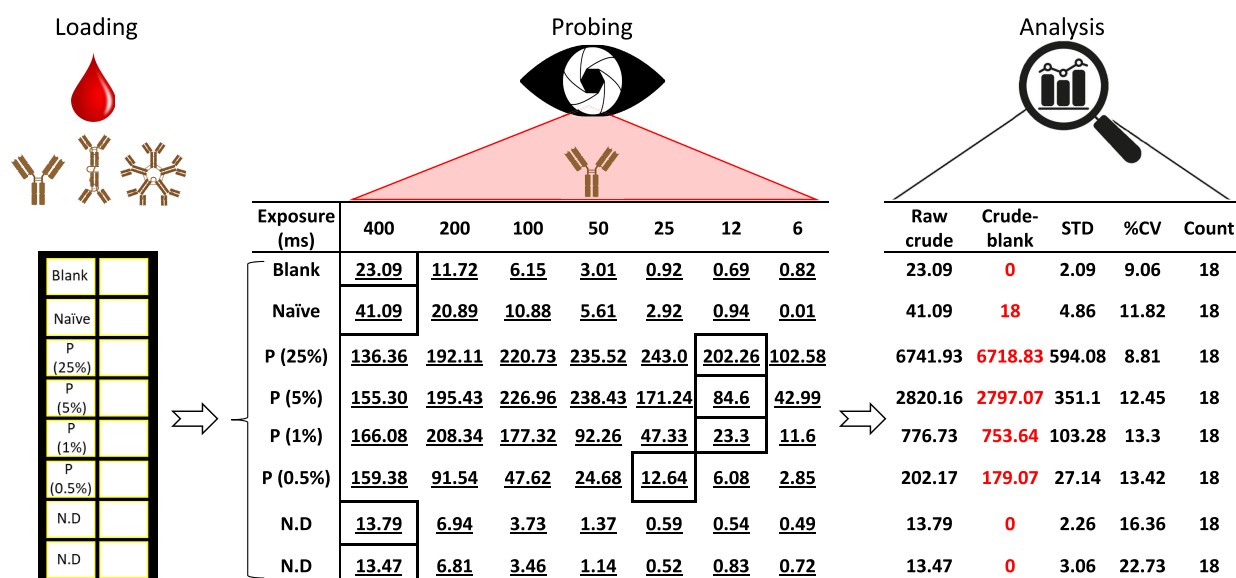


Figure 1. Quantification methodology. SARS-CoV-2 positive serum (P), negative control (naïve pre-pandemic sera), and reagent control (Blank) were loaded each in a single sub-array spotted with recombinant S2P, RBD, and NC. The positive serum was diluted as indicated (0.5–25% of sample volume). No samples were loaded on the lower end of the slide (N.D.). After probing with fluorescence-labeled secondary anti-human IgG, IgM, and IgA antibodies, the slide was scanned at three wavelengths (625, 470, and 535 nm), and the average MFI values for each antigen (18 spots) were collected at different exposure times (6–400 ms). Depicted are the results against S2P at a wavelength of 625 nm (IgG) for all exposure times. Calculated MFI values (“raw crude”) for each sample were generated from boxed values (chosen according to guidelines outlined in the Experimental Section) for each sample. For each data point, the standard deviation (STD), coefficient of variance (%CV), number of spots used for analysis (count), and blank (reagent control) subtracted values (indicated in red) were generated.

discrimination as only infected individuals undergo seroconversion on the NC.

In order to apply the developed test during clinical trials, it was important to improve the quantitative capability of the developed array. Moreover, it was crucial to ensure that assay parameters, i.e., linearity, dynamic range, specificity, accuracy, and precision, comply with predetermined specifications in order to guarantee the reproducibility of the assay’s results, both within and between tests/studies, and to enable acceptance of the data by regulatory agencies. To face these challenges and to enable determination of a comprehensive picture of vaccine immunogenicity, the aims of the present work were as follows: (i) improve the quantitative capability and dynamic range of our serological microarray while preserving its multi-component capability (detecting IgG, IgA, and IgM targeting S2P, RBD, and NC) and (ii) assess the analytical performance of the assay (compared to the WHO qualified international standard for immunoglobulins), thereby ensuring reproducibility, accuracy, and precision of the assay’s results. Here, we present the development of a novel multi-component quantitative analysis methodology and the evaluation of its analytical performance in the context of the developed array. We further present the feasibility of the developed methodology for seroconversion analysis and immunoglobulin quantification of sera from naïve and qRT-PCR SARS-CoV-2 positive individuals.

EXPERIMENTAL SECTION

Antigens. SARS-CoV-2 recombinant proteins S2P, RBD, and NC were designed, expressed, and purified as described in detail previously.^{8,9}

Clinical Samples. qRT-PCR positive sera samples ($n = 18$) were previously obtained from Sheba Hospital (Tel HaShomer Israel) from patients with severe symptoms (approval number

7036-20-SMC).⁵ Sera from qRT-PCR-negative volunteers ($n = 24$) were collected on April 24, 2020.⁵ A pre-pandemic commercial normal human serum preparation (Human pooled serum, Cat. 2931149, Lot. Q8441, MP Biomedicals LLT.) was used as a negative control. The first WHO International Standard for anti-SARS-CoV-2 immunoglobulin (human), NIBSC code: 20/136, was used for comparison analysis.

Serological Assays. SARS-CoV-2 antigens including S2P, RBD, and NC (1 mg/mL) were spotted separately, as single 300 μ L drops, in 18 repeats on 16-pad (16 sub-arrays) nitrocellulose-coated slides (Grace Bio Labs, GBL, Bend, OR) using a non-contact Piezo dispensing microarray spotter (Scienion Inc., Berlin, Germany). Slides were blocked with blocking buffer (0.1% Tween 20, 3.3% BSA in PBS) for 30 min at room temperature, washed (Tween 0.1%, 5% Bovine Serum Albumin (BSA) in PBS), dried, and stored desiccated until use. Sera, diluted (1:50 or at the indicated concentrations) in array buffer (0.1% Tween 20, 1% BSA in PBS) to a final volume of 90 μ L, were loaded (80 μ L) on the slides’ sub-arrays. Incubations were carried out for 30 min at room temperature on a plate shaker. Following incubation, the slides were washed thrice with 100 μ L of PBT (Tween 0.1% in PBS) and incubated (as described) with a detection mixture containing three fluorescently labeled secondary antibodies: Alexa647-Donkey-anti-Human IgG (H + L) (Jackson Immuno Research, West Grove, Pennsylvania, USA, 709-605-1499), Alexa488-Goat-anti-Human IgMFC5 μ (Jackson 109-545-043), and DyLight550 Rabbit-anti-Human IgA (Abcam, Cambridge, United Kingdom, ab97000), diluted (1:1000, 1:350, and 1:300 respectively) in array buffer. The slides were washed as described and dried. Slides were scanned at three different wavelengths (470, 625, and 535 nm), using a SciReader FL2 system (Scienion Inc.) and the median fluorescence intensity (MFI) for each spot at several exposure times (6, 12, 25, 50,

100, 200, and 400 ms) was recorded using Scienion scanArray software.

Data Analysis and Statistical Evaluation of Diagnostic Performance. Each slide contains 16 sub-arrays, allowing analysis of up to 16 samples. Three of these sub-arrays are dedicated to controls: a reagent control (blank), a negative control (a pool of naïve, pre-pandemic sera), and a positive control (qRT-PCR positive serum). Each sample (including the three controls) is scanned at multiple wavelengths ($w = 470, 625, \text{ and } 535 \text{ nm}$, corresponding to the anti-IgM, -IgG, and -IgA reporting antibodies, respectively) using different exposure times ($e = 6, 12, 25, 50, 100, 200, \text{ and } 400 \text{ ms}$), yielding values for every spot (data point) on the slide ($s = 1$ through 18 spots per antigen, i.e., S2P, RBD, and NC). Thus, each antigen–antibody–exposure time combination has a group of 18 data points, individually presented as three-dimensional vectors: $S[w][e][s]$. Final “Raw-crude” and “Crude-blank” median fluorescent intensity (MFI) values for each combination (for example, see Figure 1) are calculated for a given $S[w]$ applying a dedicated python script as described by the following steps:

1. For each $S[w][e]$, the standard deviation (STD), mean (Avg), and coefficient of variation (CV) are calculated for all 18 data points [$s (1-18)$] for each antigen.
2. For each $S[w][e]$, outlier casting is performed. Individual data points in [s] are declared as invalid if the Euclidian distance to the mean is larger than 2 STD while maintaining at least 14 values. If less than 14 valid values are provided (<78%) as input (the scanning software may invalidate some of the spots), $S[w][e]$ is declared as “not determined” (N.D).
3. If the mean MFI value of one of the two longest exposures (400 and 200 ms) is <60, this value is assumed to be in the linear range of the sensor. This value and the next, shorter exposure value are chosen, skipping step 4.
4. For a maximum CV (cv_max), ranging iteratively from 5 to 35% in steps of 5%, each $S[w]$ is searched for every possible couple of succeeding exposures $S[w][e_n]$ and $S[w][e_{n+1}]$ (longer and shorter, respectively), where none of the values is N.D. For each couple, the linearity coefficient error (L_i) is calculated as:

$$L_i = \left| \log\left(\frac{e_n}{e_{n+1}}\right) - \log\left(\frac{S[w][e_n]}{S[w][e_{n+1}]}\right) \right| \quad (1)$$

Couples are considered only if the CV for both exposures is smaller than cv_max . The couple where L_i is minimal is chosen, except that L_i must be smaller than $\log(2/3)$. Once such couple is found, iteration over cv_max values is ceased. If a CV larger than 25% exists in one of the chosen exposures, this fact is marked alongside the results.

If none of the succeeding [e] values satisfy the requirements, N.D is returned for the given $S[w]$. Else, the “Raw-crude” value for $S[w]$ is the expected absorbance value for $e = 400$, as extrapolated under the assumption of linearity at the higher chosen exposure, such as

$$\text{Raw - crude} = \frac{400[ms] \times S_i}{e[ms]} \quad (2)$$

where e is the length of the (longer) chosen exposure and S_i is the mean MFI value for that exposure.

5. Each $S[w]$ is compensated for the signal overlap between the emission spectra of the different fluorophores by subtracting a predetermined percentage (Table S1) of a given $S[w]$ from the other $S[w]$ received for the same sample, as indicated in the table. This percentage was determined by separately analyzing a positive sample with each of the reporter antibodies and determining the MFI signals at all the three above mentioned wavelengths, thus establishing the “leakage” between channels.
6. The Raw-crude value found for the control blank sample at each wavelength (for $e = 400 \text{ nm}$) is subtracted from every Raw-crude value in the same array and wavelength to generate “Crude-blank” values for each $S[w]$.

Acceptance ranges and limits of detection and quantification (established as exemplified in the Results section) are also embedded in the python algorithm.

Evaluations of intra- and inter-precision of the developed array and analysis algorithm were carried out using one-way analysis of variance (ANOVA) followed by Dunn’s multiple-comparison test applying GraphPad Prism 6 (La Jolla, CA). Sensitivity, specificity, positive predictive values (PPV), and negative predictive values (NPV) were calculated using the contingency tables option of GraphPad Prism 6.

Ethics Statement. Sample collection was approved by the SMC institutional review board committee for broad antibody testing (approval number 7036-20-SMC). The patients gave their written informed consent before the examination was performed. The relevant regulations and institutional policies were followed strictly.

RESULTS

Development of a Novel Algorithm for Antibody Quantitation. Fluorescence-based serological microarrays enable simultaneous determination of several antibody isotypes in a tested serum by means of discrete fluorescently labeled secondary antibodies. Results are generated by scanning the test slide at different wavelengths, thereby generating separate signals for each of the secondary antibodies incorporated in the test. The immunoglobulin signals are determined simultaneously on each of the slide spotted antigens, whose number might reach a few dozen (The test flow of the serological microarray applied in this study is demonstrated in Figure S1). Generally, only one exposure scan time is selected,¹⁰ where long exposures favor low antibody containing samples, enhancing sensitivity while lowering the dynamic range, and short exposures differentiate between high antibody containing samples whilst lowering the assay’s sensitivity. Therefore, to enable accurate quantitation utilizing fluorescence, attaining both sensitivity and a dynamic range, one has to analyze several dilutions of the same sample, thereby rendering the methodology unsuitable for high-throughput applications. To overcome this limitation, we utilized the scanner’s ability to generate data for different exposure times (6–400 ms) for each spotted antigen for each antibody isotype, in our case, determining IgG, IgM, and IgA bound to SARS-CoV-2 antigens: S2P, RBD, and NC. A dedicated novel algorithm then generates a calculated fluorescence signal for each test (a total of nine tests: three antigens \times three antibody isotypes), computed from the linear range of the mean fluorescence intensity (MFI) values collected at different exposure times, as explained in detail in the Experimental Section. As an example

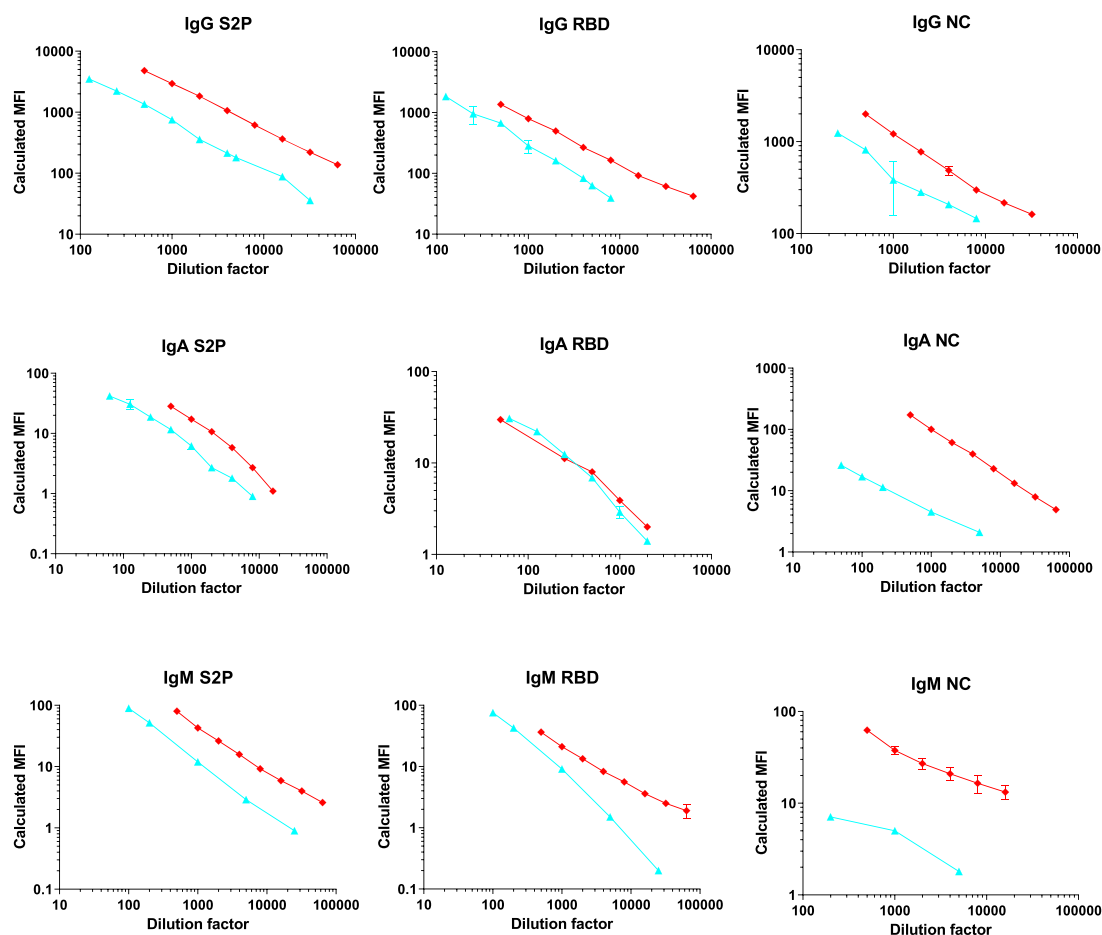


Figure 2. Linearity of the multi-component array. SARS-CoV-2 qRT-PCR positive sample (red) and WHO international standard (cyan) were loaded on the multi-component array at the indicated dilutions. The slides were then reacted with secondary fluorescent antibodies and analyzed using the novel algorithm described in the previous section (and in detail in the [Experimental Section](#)). The results are the average of two independent experiments. R^2 , calculated using non-linear regression, ranged from 0.97 to 0.99 for all depicted graphs.

of the program's output, [Figure 1](#) demonstrates the results obtained for one of the multi-component tests performed simultaneously on the array, specifically IgG titer against S2P. Similar data sheets are generated for each of the antigen–antibody combinations of the array (a total of nine discreet data sheets). The left panel of [Figure 1](#) (Loading) illustrates the slide plan, including three controls: a blank sample (reagents control, comprised of the three fluorescently labeled secondary antibodies diluted in array buffer), a negative control (naïve pre-pandemic commercial sera), and a positive control (serum from a qRT-PCR positive, severely ill, recuperating individual, which was collected and characterized previously⁵). As a proof of concept, several dilutions of the positive control serum (P) are analyzed on the slide. The middle panel (Probing) portrays the MFI signals of each sample on S2P for all exposure times. These MFI signals are calculated as the average of 18 spots that are localized on different areas of the nitrocellulose slide (each sub-array of the slide contains 18 spots of each of the three antigens: S2P, RBD, and NC).

The right panel (Analysis) portrays the calculated signals for each of the samples (based on the signals obtained for the different exposure times) as well as statistical data pertaining to the chosen signals (boxed in the middle panel) used for the calculations. Indicated in red are the final calculated signals:

“Crude-blank” (after subtraction of the blank, i.e., the reagent control signal).

As demonstrated, analyzing different dilutions of the positive sample ([Figure 1](#) middle panel), choosing 400 ms as the selected exposure time, results in similar signals, regardless of the sample's dilution factor (indicating saturation and quenching of the fluorescent signal), whereas only lower exposure times (6–25 ms) enable the emergence of dose-dependent signals. As a result, in the case of IgG signals on S2P, a lower exposure time was automatically determined as optimal. This however might not be the case for IgG signals on RBD or NC (which are analyzed simultaneously), as the concentration and affinity of the serum antibodies might differ (depending on the tested individual), resulting in the selection of a different optimal exposure time. Thus, our novel methodology, optimizing the exposure time for each of the different antigens for each antibody isotype and calculating an apparent MFI signal (as described in the [Experimental Section](#)), enables accurate quantification of the overall antibody response in the analyzed sample. Moreover, since the calculated values are then normalized to the highest exposure time (400 ms), the overall values of different antigens and antibody serotypes can then be assessed over an extended dynamic range (which is extended by almost 2 orders of magnitude compared to any single exposure time). It is important to note that this quantitative methodology does not

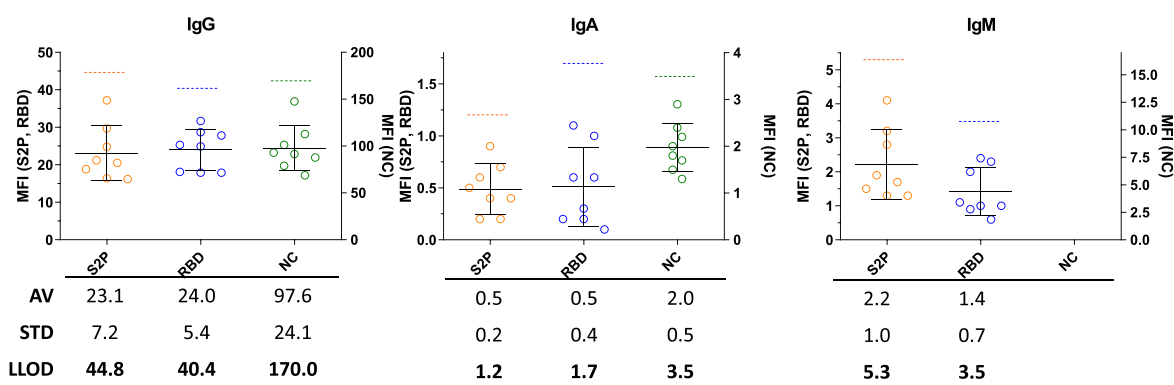


Figure 3. LLOD of the microarray tests. Upper panel: Calculated MFI values (after blank subtraction) for (left to right) IgG, IgA, and IgM signals of the commercial, pre-pandemic, naïve samples (eight independent experiments) on S2P (orange), RBD (blue), and NC (green). The average (AV), standard deviation (STD), and lower limit of detection (LLOD) for each antibody isotope for each antigen are indicated on the graph (bold black lines and dashed colored lines, respectively), and the values are presented in the lower panel. LLOD values are indicated in bold. No LLOD was determined for IgM-NC, since no acceptance range was determined for this test (due to a high CV value observed during acceptance range determination, Figure S2).

give direct classical antibody concentrations but rather relative MFI signals, embodying the complex humeral response due to exposure/vaccination.

Analytical Performance. In order to establish the feasibility of the developed methodology and to verify its suitability for routine application for evaluation of seroconversion or vaccine immunogenicity, we determined several parameters of the multi-component array, including acceptance ranges, linearity, lower limits of detection (LLOD) and quantitation (LLOQ), as well as precision and reproducibility.

Acceptance Ranges of the Assay's Controls. To enable long-term application of the methodology using different slide lots on different days, by different operators, we determined the acceptance MFI ranges for the three aforementioned controls (Figure 1): (1) a reagents control (blank) containing only secondary antibodies, (2) naïve, pre-pandemic commercial sera, and (3) a 1000-fold dilution of the positive control (P)⁵ (equivalent to 5% sample diluted in the naïve, pre-pandemic commercial sera and then diluted to 1:50 in array buffer). The results, obtained from 26 independent experiments performed by two different lab-workers, on three different slide lots and 18 different days, resulted in the determination of acceptance ranges (for the positive control) or upper acceptance limits (for the blank and negative controls) that are presented in Figure S2 and summarized in Table S2.

The qualification of a single dilution of the positive control, to be used simultaneously for all embedded tests, proved to be challenging due to the unique composition of anti-SARS-CoV-2 IgG, IgM, and IgA antibodies of the implemented serum. Coefficient of variation (CV) values were lower than 20% for IgG and lower than 30% for IgM and IgA for this positive control dilution against all tested antigens with the exception of the IgM-NC test that exhibited a higher CV value (CV = 33.5%). As a result, no acceptance range was determined for the IgM-NC test (this would have required a less diluted sample, resulting in acceptance ranges at the upper limits of the linear range for the IgG values). The three aforementioned control samples (frozen as single-use aliquots) are loaded on each slide alongside the patients/vaccinees' sera to ensure reproducibility. Slides exhibiting MFI signals ("raw crude" in Figure 1, analysis panel) that do not confirm with the indicated values (Figure S2 and Table S2) are excluded by the dedicated

analysis algorithm. All the results presented in the following sections were analyzed with the acceptance range-embedded algorithm.

Linearity and Dynamic Range. We next wanted to determine the linearity and dynamic range of the nine discreet tests performed in our multi-component array. Linearity is defined as the ability of an analytical procedure to obtain test results that are directly proportional to the concentration of the analyte in the sample. The linearity of the assay (Figure 2) was verified by serial dilutions of the SARS-CoV-2 qRT-PCR positive patient's serum (P) (as indicated, this serum, diluted to 1:1000, was also used as a positive control). This serum (Figure 2, red) displayed linear, high signals of IgG, IgA, and IgM on all the antigens spotted on the array. The serum's performance was compared to that of the WHO international standard for SARS-CoV-2 immunoglobulins (Figure 2, cyan). This standard was generated by the WHO Expert Committee on Biological Standardization with the aim of harmonizing immune response assessment after natural infection or vaccination. Both samples demonstrated a linear response that was directly proportional to the dilution factor. A different range of linear responses was displayed by each serum, depending on the humoral signature (affinity and concentration) of each specific patient/recuperating individual sample used. It is important to note, that in most cases, especially for IgA, our in-house positive control demonstrated higher values than the international standard, enabling the use of a single dilution of the sera as a positive control for all the nine discreet tests incorporated in the array. The dynamic range of all tests ranged between 2 and 3 orders of magnitude with R^2 values of 0.97–0.99 for all the developed tests (calculated using non-linear regression). As indicated in the previous section, our analysis results in relative MFI values for each sample and not actual antibody concentrations. The WHO standard was declared arbitrarily as containing 1000 antibody binding units (ABU)/mL and can be used, upon demand, to generate conversion factors that will enable a direct comparison of our assay to other assays.

Lower Limit of Detection (LLOD) and Lower Limit of Quantification (LLOQ). The LLOD of an analytical test is the lowest amount of analyte that can be detected in the sample. As per the ICH guidelines,¹¹ this value is determined as the average (AV) plus three standard deviations (STD) of a "true"

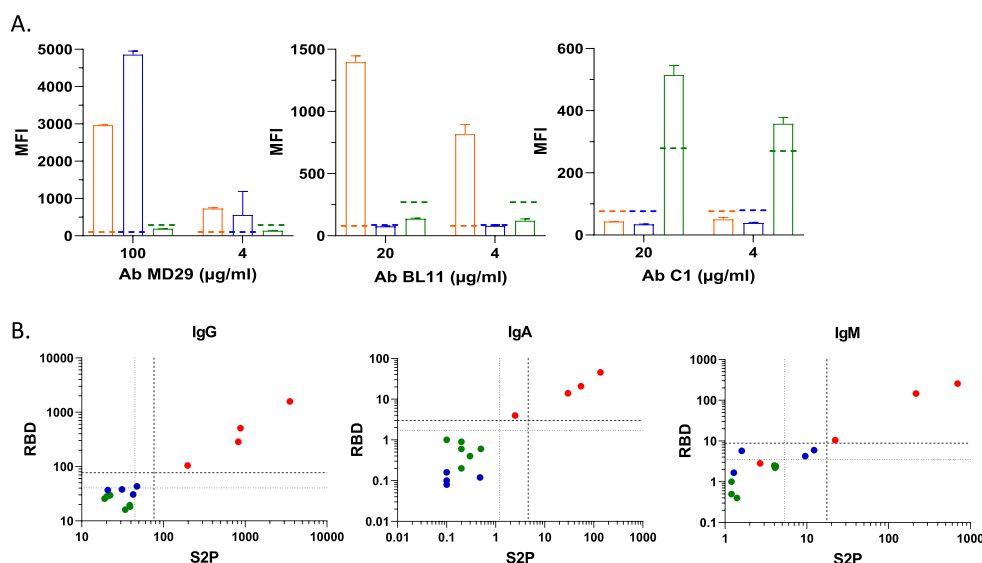


Figure 4. Assay specificity. (A) Interaction of anti-SARS-CoV-2 specific IgG monoclonal antibodies against RBD (MD29), N-terminal domain (NTD) (BL11), and NC (C1) with S2P, RBD, and NC (orange, blue, and green columns, respectively). The antibodies were loaded at the indicated concentrations. LLOQ values (Table S3, IgG) for each of the antigens are indicated with colored dashed lines (orange, blue, and green for S2P, RBD, and NC, respectively). (B) MFI values of anti-RBD vs anti-S2P antibodies for, left to right, IgG, IgA, and IgM for six independent repetitions of the pre-pandemic commercial sera (green) and four random naïve qRT-PCR negative (blue) and qRT-PCR positive (red) sera that were diluted to 1:50 in assay buffer. Some repetitions of the commercial sera are not presented on the graphs because they displayed zero signals. Dotted and dashed lines represent the assay's LLOD and LLOQ, respectively.

negative sample, in this case, the commercial naïve pre-pandemic sera. LLOD values (Figure 3) were generated from MFI signals (after blank subtraction, i.e., “raw-blank”) collected from eight independent experiments (no LLOD was determined for IgM-NC, since no acceptance range was determined for this test, Figure S2).

The LLOQ is the lowest point in the linear range (Figure S2), above the LLOD, for which quantitative values of the analyte can be extracted. This value was determined as the lowest point that can be measured with adequate accuracy ($CV < 25\%$) and represents the lowest amount of analyte that can be determined quantitatively. LLOQ values were calculated from three independent repetitions of a single positive control concentration (each of which is the average of 18 desecrate spots for each antigen), as specified in Table S3 (LLOQ values are indicated in red). For analysis, sera presenting values below the LLOQ were designated as negative (and were marked as $<LLOQ$). The LLOQ values for each single assay were also embedded in the dedicated analysis algorithm and used as cutoff values for negative/positive determination.

Specificity. To ascertain the specificity of the developed array, we implemented three previously developed monoclonal antibodies against SARS-CoV-2's RBD, NTD (Spike's N-terminal domain), and NC.^{8,9} The interaction of the monoclonal antibodies with each of the spotted antigens (orange, green, and blue for S2P, RBD, and NC, respectively) is presented in Figure 4A. For each antigen, the determined LLOQ values (Table S3) are indicated by dashed lines (colored as specified for each antigen). As expected, BL11 (Figure 4A, middle panel), an anti-NTD antibody, reacted only with the stabilized version of the SARS-CoV-2 spike ectodomain spotted on the array but not with the NC or the RBD. Similarly, C1 (Figure 4A, right panel), an anti-NC antibody, reacted only with the spotted NC but not with both spike-based antigens. Finally, MD29 (Figure 4A, left panel), an anti-RBD antibody, reacted with both spike-based moieties but

not with the NC. As indicated, all the positive and negative values of the analyzed antibodies fall within the LLOQ constrains, thus validating the specificity of the array. All the antibodies demonstrated a dose–response relationship.

Another aspect of assay specificity is defined as the assay's ability to correctly identify non-infected individuals, i.e., displays no false positive results. In this respect, our working hypothesis was that the commercial naïve pre-pandemic sera represent the background signal of people that were exposed to several unknown diseases (excluding SARS-CoV-2) and as such can be used to ascertain the assays' specificity. We therefore determined the MFI signals of three independent repetitions of this sample on two different slide lots (Figure 4B, green dots, $n = 6$). We further evaluated the specificity by applying random qRT-PCR positive and negative samples from a previous study.⁵ These samples consisted of four qRT-PCR positive patients/recuperating individuals (Figure 4B, red dots, $n = 4$) and four qRT-PCR negative volunteers (Figure 4B, blue dots, $n = 4$), whose sera were collected at the very early stages of the COVID-19 pandemic in Israel (April 2020) and are thus considered naïve. Figure 4B shows highly correlated anti-RBD versus anti-S2P MFI values for IgG, IgA, and IgM antibodies. Samples falling below the LLOQ (Dashed lines) are considered negative, whereas samples falling outside this region are considered positive. The IgG, IgM, and IgA values of all but one positive individual fall in the positive zone, probably indicating that while the IgG antibodies of this patient fall in the positive zone, his IgM and IgA antibodies already decayed or were very low to begin with as this patient displayed very mild SARS-CoV-2 symptoms.⁵ It is also possible that due to variability between individuals, this positive subject displays lower IgM/IgA values. All pre-pandemic (green dots) and naïve samples (blue dots) fall below the LLOD and LLOQ defined limits, indicating the high specificity of the developed array.

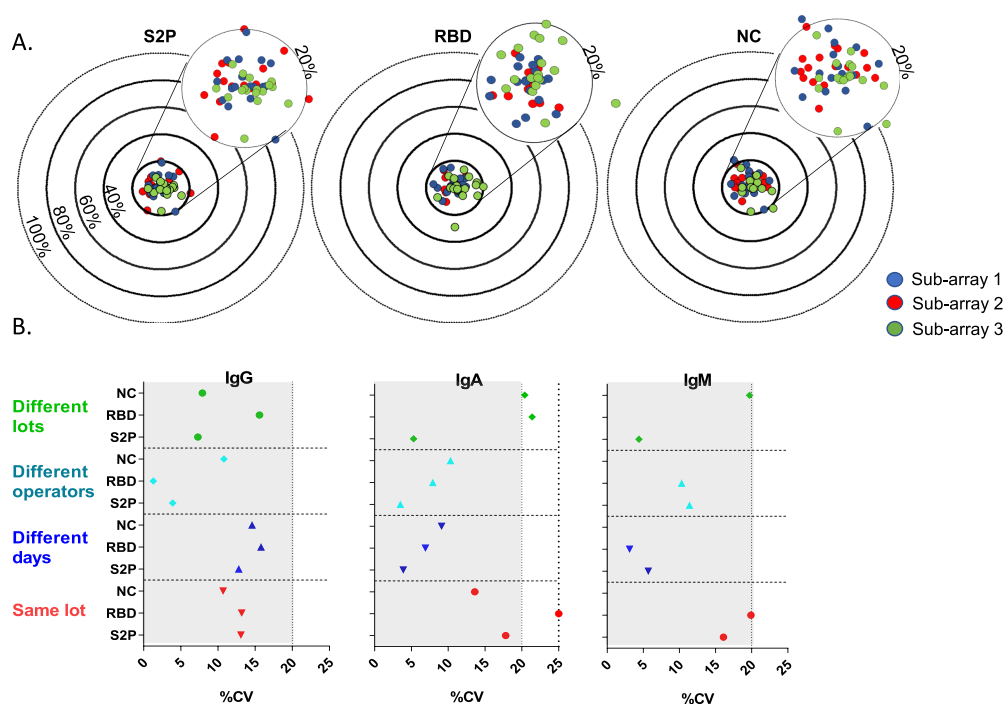


Figure 5. Assay precision. qRT-PCR positive control (diluted to 0.4, 2, and 10% dilutions for S2P, RBD, and NC, respectively) was loaded in triplicates on slides from two different lots. (A) Bullseye charts of intra-assay precision, calculated as the percent deviation (% deviation) of the MFI signals of 3×18 distinct (from left to right) S2P, RBD, or NC spots from three different sub-arrays (red, blue, and green) within the same lot, from the overall average of the spots (A total of 54 spots for each antigen). Circles (from outside to inside) indicate 100, 80, 60, 40, and 20% deviation, respectively. (B) Inter-assay precision was determined as the CV of the calculated MFI signals of triplicates within 2 slides of the same lot (red), when performed on different days (blue), when performed by different operators (cyan), and when utilizing different lots (green).

Precision and Interference. Precision portrays the degree of scatter among several measurements of the same sample, taken under different pre-determined conditions. Precision can be determined at several levels in this assay: within a single slide (intra-assay), between slides of the same lot, between days, between operators, and between slides from different lots (inter-assay). To assess intra-assay precision, we evaluated the dispersion of the MFI values within a single sub-array (18 spotted dots for each antigen) and between three different sub-arrays within a slide. To this end, we calculated the deviation from the average of a single dilution of the positive control (0.4, 2, and 10% dilution for S2P, RBD, and NC, respectively), which was loaded in triplicates on the same slide. Figure 5A depicts bullseye charts of the percent deviation (% deviation) of the MFI signals of 18 distinct S2P, RBD, or NC (left to right) spots from three different sub-arrays (red, blue, and brown) from the overall average (of the total 54 dots for each antigen). Results indicate that most of the values (>96%) fall within the 20% difference limit and despite some irregular values, the CVs within each sub-array and within the slide itself comply with the acceptance criteria of $CV < 20\%$, for all the antigens. It is important to note that when outliers do exist, they are excluded from the calculations, as long as at least 14/18 spots are considered valid (see the Experimental Section for valid spot criteria). To evaluate inter-assay precision, two different operators on two different days loaded the same pre-determined positive control dilutions in triplicates on same/different slide lots. The %CV was calculated for the six resulting MFI values for each parameter (for example: three triplicates of a single dilution for each of the two operators), where each value was calculated (applying the novel algorithm) as the average of 18 dots that exhibited CV

$< 20\%$, as indicated in the intra-assay qualification. Results for the three individual antigens (Figure 5B) indicate that all the calculated CVs fall within an acceptable range, with IgG and IgM assays demonstrating $CV < 20\%$ (as indicated previously, the IgM-NC test was decreed as irrelevant) and IgA $CV < 25\%$. Interference is defined as the relative error (RE) between a predetermined value and an observed value. To assess the assay's interference, we chose two different strategies. In the first one, monoclonal antibody MD29 (that was applied to determine the assay's specificity) was diluted and reacted with the multi-component array (Figure S3A). The generated dose–response curves were then used to calculate the apparent antibody concentrations ($\mu\text{g}/\text{ml}$) of both the WHO international standard and the in-house positive control from the predetermined MFI values for each antigen. The resulting values were then compared to the expected dilution-factor-based values. In the second strategy, we determined the expected MFI values of three patient samples, across the working range of the array. The observed versus expected values for the three samples for IgG on S2P and RBD were then determined on two independent slide lots (Figure S3B). For both strategies, all RE values were lower than $\pm 30\%$ with $\%CV < 20$, demonstrating the quantitative capability of the array.

Quantifying Anti-SARS-CoV-2 Antibodies in Patients and Naive Samples. The application of the qualified array to patients/naive sera was carried out with qRT-PCR negative and positive samples that were collected at the beginning (March–April 2020) of the COVID-19 pandemic in Israel⁵ and were analyzed in our previous work. Scatterplots of individual MFI values (calculated by applying the novel analysis algorithm) for IgG, IgM, and IgA for positive (P)

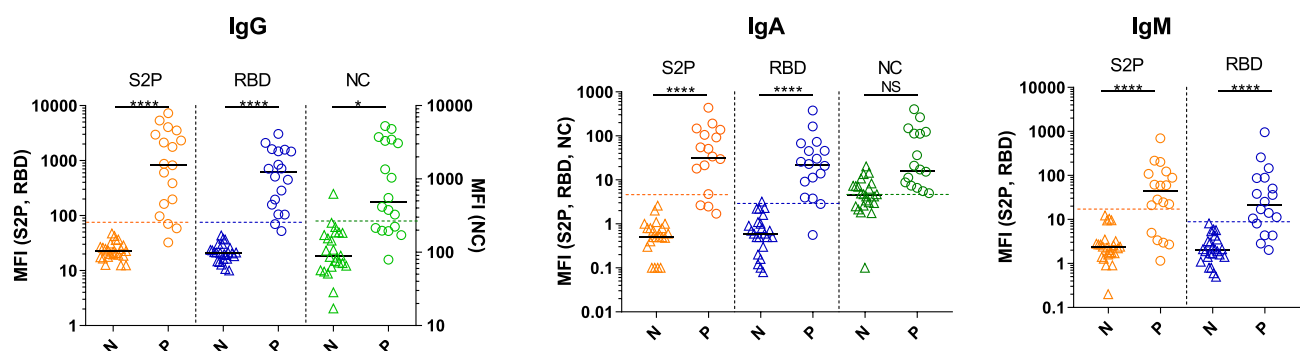


Figure 6. Scatterplot of MFI values of qRT-PCR-positive and -negative sera on the SARS-CoV-2 multi-component array. Left to right: IgG, IgA, and IgM signals of qRT-PCR-negative (N; triangles) and -positive (P; circles) sera, analyzed on S2P (orange), RBD (blue), and NC (green). The distribution of the signals obtained from individual positive/negative serum samples is presented for each antigen. Horizontal black lines indicate the median value for each set. Dashed colored lines represent the LLOQ of each test. Statistical analysis was performed using one-way ANOVA followed by Dunn's multiple-comparison test, using GraphPad Prism 6. ****, $P < 0.0001$; *, $P < 0.05$; NS, not significant.

versus negative (N) sera for S2P, RBD, and NC are presented in Figure 6. Significant fluorescence signals (p values < 0.0001) were obtained with positive sera samples for IgG, IgA, and IgM against S2P and RBD. For NC, only IgG anti-NC antibodies were found to be significantly different (p value < 0.05) than those obtained from naïve individuals. These results demonstrate the feasibility of the multi-component array for differentiating between naïve and seroconverted individuals, based on IgG signals on both the spike and the NC. In all cases, sensitivity was traded for higher specificity (sensitivity, specificity, positive predictive values (PPV), and negative predictive values (NPV) for the nine discrete array's tests are summarized in Table S4), resulting in very high PPVs and somewhat lower NPVs. In the assay's setup (tested sera diluted to 1:50), the NC-antigen, specifically IgA signals against NC, seems to be the least suitable indexes for seroconversion. This result is in agreement with the assay's directive; as for vaccine assessment, the NC is supposed to indicate exposure to the virus and is not part of the humoral response following vaccination.

DISCUSSION

To improve the quantitative capability of our multi-component serological array, we developed a novel algorithm, where quantitation is achieved by analyzing different exposure times of fluorescence-based readouts, instead of analyzing several dilutions of a sample, as is generally done in ELISA assays. This methodology utilizes the "linear range" of the exposure-induced fluorescence to calculate an MFI value proportional to the serum's antibody concentration and affinity against predetermined SARS-CoV-2 antigens. This methodology resulted in extended dynamic ranges for all targets, enabling simultaneous generation of the overall humoral response of an individual from a single sub-array. While other technologies such as SIMOA¹² and Luminex¹³ demonstrate high precision, extended dynamic ranges, and simultaneous detection of several analytes, they do not facilitate multiplexing of the reporting moieties for the same antigen (in this case, simultaneous detection of all three immunoglobulin types), thus imposing the implementation of three independent tests per sample in such a scenario. The scanner implemented in this study was an inexpensive, compact (computer sized) benchtop light-emitting-diode (LED)-based scanner. As mentioned, this scanner facilitates scanning at three distinct wavelengths with the only drawback of suffering from a

somewhat limited dynamic range. Our algorithm exploited the scanner's ability to generate results at different exposure times, allowing the computational extension of the dynamic range and quantitation accuracy while preserving the test's multiplexing capacity. Such an algorithm can be applied to improve the dynamic range and quantitation capability of other fluorescence-based tests.

We next demonstrated that the developed multi-component microarray, combined with the analytical algorithm, shows excellent reproducibility, with intra- and inter-assay variabilities falling within acceptable limits of precision. The predetermined acceptance ranges ensured batch-to-batch and operator-to-operator consistency, allowing for ongoing comparison of different time points along the vaccination process for each individual. The performance of the array was verified with the WHO first international standard (IS), a reference serum (comprised of 11 convalescent individuals) that was introduced by the WHO Expert Committee on Biological Standardization in December 2020 with the aim of harmonizing immune response assessment after natural infection or vaccination.^{4,14} The serum was assigned an arbitrary value of 1000 units/mL for binding/neutralizing assays and can thus be used to assist in standardizing our results, compared to other assays detecting the same class of immunoglobulins with the same specificity. We recently assessed the neutralization capacity of a small subset of the vaccinated volunteers' sera against SARS-CoV-2 and several of its relevant circulating variants-of-concern, demonstrating the high potency of BriLife against the tested viruses.¹⁵ Moving forward, the binding data collected from the serological array, in combination with the neutralization data, may allow the generation of a binding/neutralizing correlate of protection for BriLife as was demonstrated for the mRNA-1273 vaccine.¹⁶

As indicated, this multi-component array was developed to evaluate the immunogenicity of BriLife, the Israeli vaccine (results will be published elsewhere, at the end of phase I/II of the clinical trial). Since the evaluation of the vaccine's immunogenicity and potency is currently ongoing, array performance was evaluated with naïve versus SARS-CoV-2-diagnosed patients. Results indicate that IgG antibodies enable sensitive and specific discrimination between naïve and SARS-CoV-2 positive individuals. As indicated (Figure 6), at the assay setup (serum samples are diluted to 1:50), some naïve individuals had NC background signals that exceeded the determined LLOQ (specifically for IgA-NC). This phenom-

enon might arise from cross-reacting antibodies due to previous exposure to circulating corona viruses as was found by us and others.^{5,17} To overcome this limitation, baseline serums of each of the individuals that are part of the clinical trial are used as background levels all through the experiment. This allows for direct discrimination between vaccinees that have undergone seroconversion due to vaccination (response on both S2P and RBD but not on NC) and those that were infected with SARS-CoV-2 (significant signal on all the tested antigens) during follow-up.

In conclusion, our multi-component assay in combination with the novel algorithm offers benefits in terms of time, cost, required sample volume, as well as multiplexing, compared to conventional immunoassays. The developed platform is similar in practice to ELISA but is customizable, can be scaled up, relies on microliter quantities of samples, and has the ability to screen sera for multiple antigens against different antibody isotypes. It is therefore particularly suitable for large-scale screening and analysis including sero-surveillance and monitoring of immune responses to vaccines.

■ ASSOCIATED CONTENT

SI Supporting Information

The Supporting Information is available free of charge at <https://pubs.acs.org/doi/10.1021/acs.analchem.1c05264>.

Word document containing (Figure S1), schematic representation of the multi-component serological test (Figure S2), scatter plots of MFI values of the assay's controls (Figure S3), expected versus observed values (Table S1), compensation for signal overlap between chromophores (Table S2), acceptance ranges and upper limits of the assay's controls (Table S3), LLOQ MFI values (Table S4), sensitivity, specificity, PPV, and NPV of the distinct multi-component array's tests (PDF)

■ AUTHOR INFORMATION

Corresponding Author

Adva Mechaly – Department of Infectious Diseases, Israel Institute for Biological Research, 7410001 Ness-Ziona, Israel; orcid.org/0000-0003-0565-6001; Email: advam@iibr.gov.il

Authors

Morly Fisher – Department of Infectious Diseases, Israel Institute for Biological Research, 7410001 Ness-Ziona, Israel
Alon Manor – Department of Environmental Physics, Israel Institute for Biological Research, 7410001 Ness-Ziona, Israel
Hagar Abramovitch – Department of Quality Assurance, Israel Institute for Biological Research, 7410001 Ness-Ziona, Israel
Ella Fatelevich – Department of Infectious Diseases, Israel Institute for Biological Research, 7410001 Ness-Ziona, Israel
Yafa Afrimov – Department of Infectious Diseases, Israel Institute for Biological Research, 7410001 Ness-Ziona, Israel
Gal Bilinsky – Department of Biochemistry and Molecular Genetics, Israel Institute for Biological Research, 7410001 Ness-Ziona, Israel
Edith Lupu – Department of Biotechnology, Israel Institute for Biological Research, 7410001 Ness-Ziona, Israel
Amir Ben-Shmuel – Department of Infectious Diseases, Israel Institute for Biological Research, 7410001 Ness-Ziona, Israel

Itai Glinert – Department of Infectious Diseases, Israel Institute for Biological Research, 7410001 Ness-Ziona, Israel
Noa Madar-Balakirski – Department of Pharmacology, Israel Institute for Biological Research, 7410001 Ness-Ziona, Israel
Hadar Marcus – Department of Biotechnology, Israel Institute for Biological Research, 7410001 Ness-Ziona, Israel

Complete contact information is available at: <https://pubs.acs.org/doi/10.1021/acs.analchem.1c05264>

Author Contributions

The manuscript was written through contributions of all authors. All authors have given approval to the final version of the manuscript.

Notes

The authors declare no competing financial interest.

■ ACKNOWLEDGMENTS

We want to thank the CBRN Defense Division, Israeli Ministry of Defense, for their assistance in clinical samples collection.

■ REFERENCES

- (1) Bohn, M. K.; Lippi, G.; Horvath, A.; Sethi, S.; Koch, D.; Ferrari, M.; Wang, C. B.; Mancini, N.; Steele, S.; Adeli, K. *Clin. Chem. Lab. Med.* **2020**, *58*, 1037–1052. Ravi, N.; Cortade, D. L.; Ng, E.; Wang, S. X. *Biosens. Bioelectron.* **2020**, *165*, 112454.
- (2) Perkmann, T.; Perkmann-Nagele, N.; Breyer, M.-K.; Breyer-Kohansal, R.; Burghuber, O. C.; Hartl, S.; Aletaha, D.; Sieghart, D.; Quehenberger, P.; Marculescu, R.; Mucher, P.; Strassl, R.; Wagner, O. F.; Binder, C. J.; Haslacher, H. *Clin. Chem.* **2020**, *66*, 1405–1413. (accessed 8/31/2021)
- (3) Gundlapalli, A. V.; Salerno, R. M.; Brooks, J. T.; Averhoff, F.; Petersen, L. R.; McDonald, L. C.; Iademarco, M. F.; Response, C. C. *Open Forum. Infect. Dis.* **2021**, *8*, ofaa555.
- (4) Perkmann, T.; Perkmann-Nagele, N.; Koller, T.; Mucher, P.; Radakovics, A.; Marculescu, R.; Wolzt, M.; Wagner, O. F.; Binder, C. J.; Haslacher, H. *Microbiol. Spectr.* **2021**, *9*, No. e0024721.
- (5) Fisher, M.; Levy, H.; Fatelevich, E.; Afrimov, Y.; Ben-Shmuel, A.; Rosenfeld, R.; Noy-Porat, T.; Glinert, I.; Sittner, A.; Biber, A.; et al. *Microbiol. Spectr.* **2021**, No. e0087021.
- (6) Yahalom-Ronen, Y.; Tamir, H.; Melamed, S.; Politi, B.; Shifman, O.; Achdout, H.; Vitner, E. B.; Israeli, O.; Milrot, E.; Stein, D.; Cohen-Gihon, I.; Lazar, S.; Gutman, H.; Glinert, I.; Cherry, L.; Vagima, Y.; Lazar, S.; Weiss, S.; Ben-Shmuel, A.; Avraham, R.; Puni, R.; Lupu, E.; Bar-David, E.; Sittner, A.; Erez, N.; Zichel, R.; Mamroud, E.; Mazor, O.; Levy, H.; Laskar, O.; Yitzhaki, S.; Shapira, S. C.; Zvi, A.; Beth-Din, A.; Paran, N.; Israely, T. *Nat. Commun.* **2020**, *11*, 6402.
- (7) Bal, A.; Pozzetto, B.; Traubad, M.-A.; Escuret, V.; Rabilloud, M.; Langlois-Jacques, C.; Paul, A.; Guibert, N.; D'Aubarède-Fried, C.; Massardier-Pilonchery, A.; et al. *Clin. Chem.* **2021**, *67*, 742–752. (accessed 8/31/2021). Bonelli, F.; Sarasini, A.; Zierold, C.; Calleri, M.; Bonetti, A.; Vismara, C.; Blocki, F. A.; Pallavicini, L.; Chinali, A.; Campisi, D.; et al. *J. Clin. Microbiol.* **2020**, *58*, e01224–e01220. Padoan, A.; Bonfante, F.; Pagliari, M.; Bortolami, A.; Negri, D.; Zuin, S.; Bozzato, D.; Cosma, C.; Sciacovelli, L.; Plebani, M. *EBioMedicine* **2020**, *62*, 103101. Suhandynata, R. T.; Hoffman, M. A.; Huang, D.; Tran, J. T.; Kelner, M. J.; Reed, S. L.; McLawhon, R. W.; Voss, J. E.; Nemazee, D.; Fitzgerald, R. L. *Clin. Chem.* **2021**, *67*, 404–414. (accessed 6/10/2021) Tang, M. S.; Case, J. B.; Franks, C. E.; Chen, R. E.; Anderson, N. W.; Henderson, J. P.; Diamond, M. S.; Gronowski, A. M.; Farnsworth, C. W. *Clin. Chem.* **2020**, *66*, 1538–1547. (accessed 8/31/2021) Patel, E. U.; Bloch, E. M.; Clarke, W.; Hsieh, Y.-H.; Boon, D.; Eby, Y.; Fernandez, R. E.; Baker, O. R.; Keruly, M.; Kirby, C. S.; Klock, E.; Littlefield, K.; Miller, J.; Schmidt, H. A.; Sullivan, P.; Piwowar-Manning, E.; Shrestha, R.; Redd, A. D.; Rothman, R. E.; Sullivan, D.; Shoham, S.; Casadevall, A.; Quinn, T. C.; Pekosz, A.; Tobian, A. A. R.; Laeyendecker, O. J. *Clin. Microbiol.*

2021, 59, e02257–e02220. Corbett Kizzmekia, S.; Nason Martha, C.; Flach Britta, G. M.; O'Connell Sarah, J. T. S. *Science* **2021**, 373, No. eabj0299.

(8) Barlev-Gross, M.; Weiss, S.; Ben-Shmuel, A.; Sittner, A.; Eden, K.; Mazuz, N.; Glinert, I.; Bar-David, E.; Puni, R.; Amit, S.; et al. *Anal. Bioanal. Chem.* **2021**, 413, 3501–3510.

(9) Noy-Porat, T.; Makdasi, E.; Alcalay, R.; Mechaly, A.; Levy, Y.; Bercovich-Kinori, A.; Zauberman, A.; Tamir, H.; Yahalom-Ronen, Y.; Israeli, M.; Epstein, E.; Achdout, H.; Melamed, S.; Chitlaru, T.; Weiss, S.; Peretz, E.; Rosen, O.; Paran, N.; Yitzhaki, S.; Shapira, S. C.; Israely, T.; Mazor, O.; Rosenfeld, R. *Nat. Commun.* **2020**, 11, 4303.

(10) Jaeschke, A.; Eckert, H.; Bray, L. J. *BMC Bioinformatics* **2020**, 21, 72. Khan, S.; Jain, A.; Taghavian, O.; Nakajima, R.; Jasinskas, A.; Supnet, M.; Felgner, J.; Davies, J.; de Assis, R. R.; Jan, S.; Obiero, J.; Strahsburger, E.; Pone, E. J.; Liang, L.; Davies, D. H.; Felgner, P. L. *J. Visualized Exp.* **2019**, 149, No. e59973. From NLM

(11) Borman, P.; Elder, D. Q2(R1) Validation of Analytical Procedures. In *ICH Quality Guidelines*; John Wiley & Sons: 2017, pp. 127–166.

(12) Ogata, A. F.; Maley, A. M.; Wu, C.; Gilboa, T.; Norman, M.; Lazarovits, R.; Mao, C.-P.; Newton, G.; Chang, M.; Nguyen, K.; et al. *Clin. Chem.* **2020**, 66, 1562–1572. (accessed 11/3/2021)

(13) Dobano, C.; Vidal, M.; Santano, R.; Jimenez, A.; Chi, J.; Barrios, D.; Ruiz-Olalla, G.; Rodrigo Melero, N.; Carolis, C.; Parras, D.; et al. *J. Clin. Microbiol.* **2021**, 59, No. e01731.

(14) Infantino, M.; Pieri, M.; Nuccetelli, M.; Grossi, V.; Lari, B.; Tomassetti, F.; Calugi, G.; Pancani, S.; Benucci, M.; Casprini, P.; et al. *Int. Immunopharmacol.* **2021**, 100, 108095.

(15) Yahalom-Ronen, Y.; Erez, N.; Fisher, M.; Tamir, H.; Politi, B.; Achdout, H.; Melamed, S.; Glinert, I.; Weiss, S.; Cohen-Gihon, I.; et al. *Vaccines* **2022**, 10 (2), 291.

(16) Gilbert, P. B.; Montefiori, D. C.; McDermott, A. B.; Fong, Y.; Benkeser, D.; Deng, W.; Zhou, H.; Houchens, C. R.; Martins, K.; Jayashankar, L.; et al. *Science* **2021**, No. eab3435.

(17) Dobano, C.; Santano, R.; Jimenez, A.; Vidal, M.; Chi, J.; Rodrigo Melero, N.; Popovic, M.; Lopez-Aladid, R.; Fernandez-Barat, L.; Tortajada, M.; et al. *Transl Res* **2021**, 232, 60–74. Hicks, J.; Klumpp-Thomas, C.; Kalish, H.; Shunmugavel, A.; Mehalko, J.; Denson, J. P.; Snead, K. R.; Drew, M.; Corbett, K. S.; Graham, B. S.; et al. *J Clin Immunol* **2021**, 41, 906–913.